Unoccupied electronic states of Au(113): Theory and experiment

Patricio Häberle,[1,*] Wladimir Ibañez,[1] Rolando Esparza,[1] and Patricio Vargas[1,2]
[1]*Departamento de Física, Universidad Técnica Federico Santa María, Casilla 110-V,Valparaíso, Chile*
[2]*Departamento de Física, Universidad de Santiago de Chile, P.O. Box 307, Santiago-2, Chile*
(Received 5 June 2000; revised manuscript received 10 October 2000; published 30 May 2001)

We present results from inverse photoemission spectroscopy in the isochromat mode, with angular resolution, from a clean Au(113) surface. To identify the origin of the different resonances, we have performed a first-principles calculation of the bulk band structure in the linear-muffin-tin-orbital formalism. We predict the dispersion of the bulk features, as a function of parallel momentum, considering energy and momentum conservation. We have been able to identify unambiguously two surface resonances and a surface state in the $[\bar{1}10]$ and $[33\bar{2}]$ directions, respectively, as well as various bulk-derived features.

DOI: 10.1103/PhysRevB.63.235412 PACS number(s): 73.20.At

I. INTRODUCTION

The electronic structure of the low-index faces of noble metals has been the subject of many experimental studies using techniques such as photoemission, two-photon photoemission, and inverse photoemission. Several of these studies dealt with the electronic structure above the Fermi level[1–6] (ε_F). The main interest has been in the description of image states and resonances together with the identification of crystal-derived surface states.[7]

For Au(100), for example, there are data confirming the existence of a surface state within the band gap at $\bar{\Gamma}$,[8,9] and also a couple of bulk-derived surface resonances along the $\bar{X}\bar{\Gamma}\bar{M}$ directions. Similarly Au(111) shows a resonance which has been assigned to an image state at an energy above the band gap at $\bar{\Gamma}$.[9,10] On Au(110),[11] for energies above ε_F, there are two surface states at $\bar{X}$ and one at $\bar{Y}$ within a band gap. For low-index Au surfaces, then, in every band gap at least one surface state has been detected; image states have been observed, even if the states are within the bulk-allowed energy-momentum region. All these surfaces have in common that they show a room-temperature reconstruction, but little effect from this has been detected in the empty electronic states. The results presented below are no exception to this general rule.

Au is still a subject of interest as a fairly inert substrate to grow thin films of ferromagnetic materials[12] that display oscillatory magnetization. An important aspect in the growth of these very thin films is the mismatch between the lattice parameters of the substrate and the film. Both the morphology of the growth, and therefore the physical properties of the films, are strongly dependent on this parameter. In the search for the proper growth orientation and mass density of the epitaxial layers, vicinal surfaces such as fcc(113) could be considered, but there is a lack of both experimental and theoretical descriptions of their electronic structure. In the case of thin films,[13,14] both the width and intensity of the unoccupied adsorbate induced resonances have been shown to depend on the details of the substrate electronic structure.

In the present study we describe the unoccupied electronic states of Au(113) along the two principal axes of this surface. We used inverse photoemission spectroscopy (IPS) together with first-principles calculations of the bulk band structure, to provide a complete interpretation of the origin and nature of the different resonances present in our measurements. This numerical-experimental combination should prove valuable in a description of the unoccupied states of more complex systems, such as thin metallic layers over a crystalline substrate.

II. EXPERIMENT

Inverse photoemission spectroscopy is a technique which renders information regarding the unoccupied band structure of a solid[15] from ε_F up to 10 or 15 eV above, including especially the energy region below the vacuum level. Our experiments were performed in a vacuum chamber equipped with an isochromat inverse photoemission spectrometer, based on a design by Denninger *et al.*[16] The photon detector is a Geiger Müller counter filled with iodine as a discharge gas, and He as a buffer gas. The window that accepts the photons into the detector is a polished SrF_2 disc. The combination of the band gap of the window and the ionization potential of iodine makes this detector highly sensitive to photons in a very narrow band around 9.5 ± 0.3 eV.[4] The electron beam is produced by an electron gun, with a BaO cathode, based on a design by Erdman and Zipf.[17] The sample is mounted on a goniometer with both an azimuthal rotation and a rotation through an angle theta (θ) around an axis in the plane of the sample. This is an improved manipulator, which allows a much more precise and reproducible positioning than the one we used on a preliminary measurement on this same system.[18] The azimuthal angle is adjusted such that the electron momentum parallel to the surface ($\hbar k_{//}$) is oriented along a major crystallographic direction. By changing θ we can change the angle between the surface normal and the incident electronic momentum (k). A typical spectrum shows the photon intensity as a function of the energy of the incoming electrons in increments of 0.2 eV. The onset of the photon emission intensity determines the location of ε_F. A resonance in one of these spectra can be represented as a point in an energy-momentum (ε vs $k_{//}$) plot using the relation $k_{//} = \sin\theta\sqrt{(2m/\hbar^2)(\varepsilon + \hbar\omega - \phi)}$, with m being the electron mass, ε the energy of the resonance measured with respect to (ε_F), $\hbar\omega$ the energy of the detected photons, ϕ the work function of the sample [5.3 eV for Au (Ref. 19)], and θ as defined above.

The sample was prepared from 5N Au boule, which was first mechanically polished and then electropolished with the surface normal oriented within 0.5° of the [113] direction, as verified by x-ray diffraction. It was successively sputtered with a 1-keV Ar^+-ion beam, and annealed to 450 °C. The surface displays a low energy electron-diffraction (LEED) pattern consistent with a clean surface. It shows a reconstruction close to a 1×5 symmetry.[20,21] From the LEED pattern itself we cannot determine if the phase is incommensurate with the substrate, without a detailed LEED *I-V* or other structural study. A previous study of this surface using x-ray diffraction[22] showed this reconstruction to be incommensurate, but no structural model for the surface has yet been proposed.

III. NUMERICAL CALCULATION

In order to determine the origin of the electronic resonances that appear in our measurements, we performed a detailed calculation of the bulk electronic states of Au. We used the standard linear-muffin-tin-orbital technique[23] for a Au lattice in the fcc structure with $a=4.08$ Å. The calculation, in reciprocal space, considered a mesh of 18 points along each of the three primitive directions, and the use of a tetrahedron method to perform the required integrations in the first Brillouin zone. The resulting band structure along the different crystallographic directions, together with the corresponding density of states, are consistent with previous calculations.[24]

In order to facilitate the interpretation of our experimental IPS measurements, we performed a projection of the electronic states along the two main perpendicular directions of the (113) surface, namely, the $[\bar{1}10]$ and $[33\bar{2}]$ directions. In this way, we can represent in a single graph all the energy states with a common $k_{//}$, regardless of the momentum in the direction normal to the surface. Figures 1 and 2 show the projected bands along the two perpendicular directions in *k* space. Since our calculation is made in a discrete set of planes, the resulting graph still shows the underlying symmetry of the projected states. For both figures we have used a mesh of 100 points for the complete range of $k_\perp$. It is easy to recognize the existence of energy gaps between 1 and 3 eV above the Fermi energy in both directions. These gaps, in this energy region, appear in two main directions in *k* space (see Fig. 3), and therefore they can be labeled as an appropriate combination of *X* and *L* characters, with $k_X=(1,0,0)$ and $k_L=(\frac{1}{2},\frac{1}{2},\frac{1}{2})$ in units of $2\pi/a$.

To visualize the location of these energy gaps further, we calculated all the electronic states inside a cube of side $(4\pi/a)$ in reciprocal space. Figure 3 shows a constant energy surface of the electronic states between 2.5 and 3 eV above ε_F. This small energy range (0.5 eV) has been chosen to provide enough points for a suitable representation of a *constant energy surface*. This is a requirement of the smoothing and fitting routines used to generate the graph. The cube has been rotated in such a way that the [113] direction is normal to the plane of the figure. The constant energy surface shows two gaps on each axis and, in each case, they are both located symmetrically with respect to the projection of the inverse space origin onto the (113) plane $(\bar{\Gamma})$.

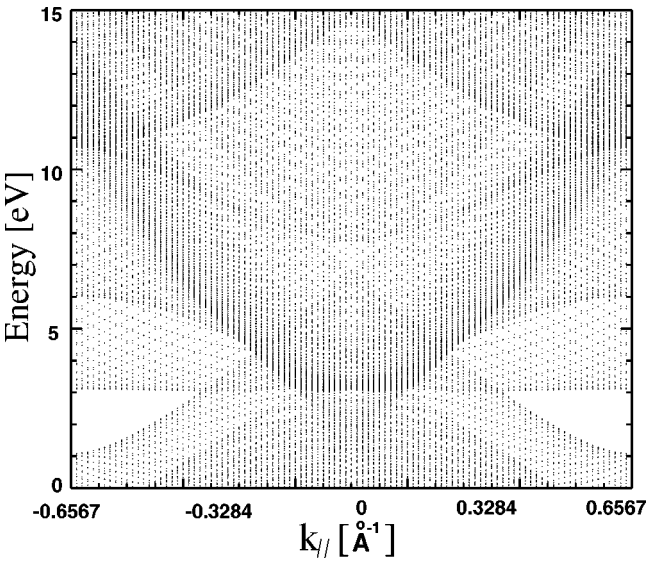

FIG. 1. Au fcc bulk band structure projected in the (113) surface along the $[33\bar{2}]$) direction in *k* space. The energy scale refers to ε_F. At the extreme of the SBZ we can see an energy band gap between 1 and 3 eV, which becomes narrower for smaller $k_{//}$ until it disappears at $k_{//}\approx0.33$ Å^{-1}.

In a complete representation of the inverse space, only the gaps shown along the $[33\bar{2}]$ direction remain. The rest of the space is filled by electronic states from other zones, with their respective centers slightly displaced. In particular the gaps along the $[\bar{1}10]$ direction disappear, and they cannot be observed in the surface-projected band structure (see Fig. 2).

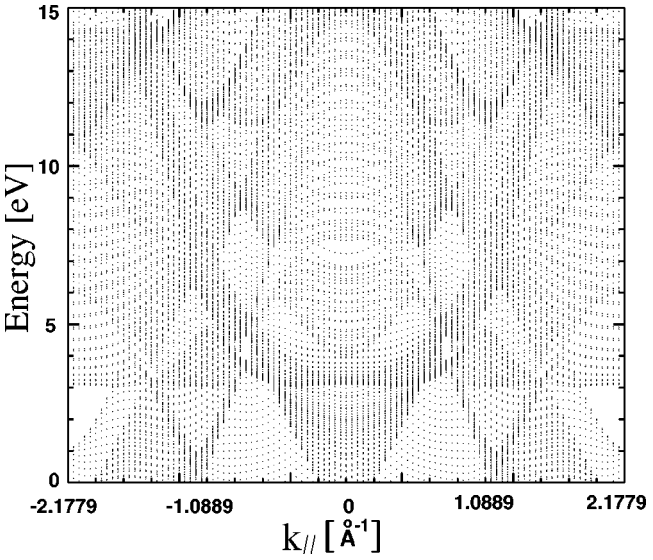

FIG. 2. Au fcc bulk band structure projected in the (113) surface along the $[\bar{1}10]$ direction. The energy scale refers to ε_F. The same band gap observed in Fig. 1 can also be reached along this direction.

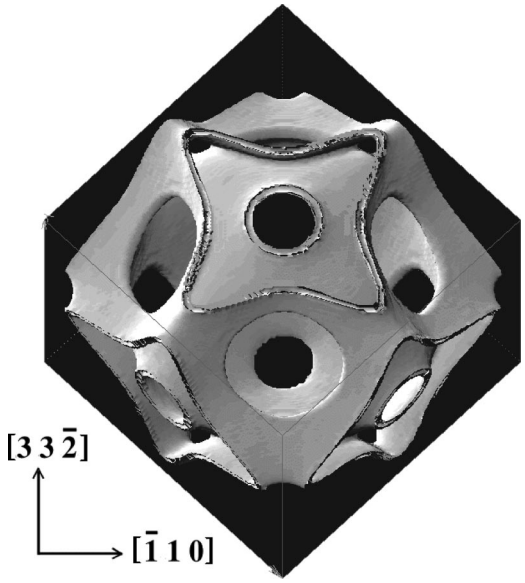

FIG. 3. *k*-space surface of constant energy for Au bulk electronic states (2.5→3.0) eV above ε_F. The [113] direction in the reciprocal lattice is normal to the plane of the figure, $\bar{\Gamma}$. The projection of the *k*-space origin is at the symmetry center of the constant energy surface. Two sets of band gaps are clearly seen in each of the main perpendicular directions. Only one of them persists (along the $[33\bar{2}]$ direction) after the electronic states are projected onto the surface.

The two gaps in the $[33\bar{2}]$ direction are also seen along the perpendicular direction, as shown by Figs. 1 and 2, simply due to the peculiar shape of surface Brillouin zone for the (113) surface (see Fig. 4). By inspection of Fig. 3, we can clearly see that the gaps in this energy region occur by a superposition in *k* space of the projections of the necks joining the neighboring cubes along the six [100] equivalent directions and the gaps in the zone boundary along the cube diagonals ([111] direction). In Sec. IV we will see how this information is relevant in the labeling of the different surface resonances as seen by IPS.

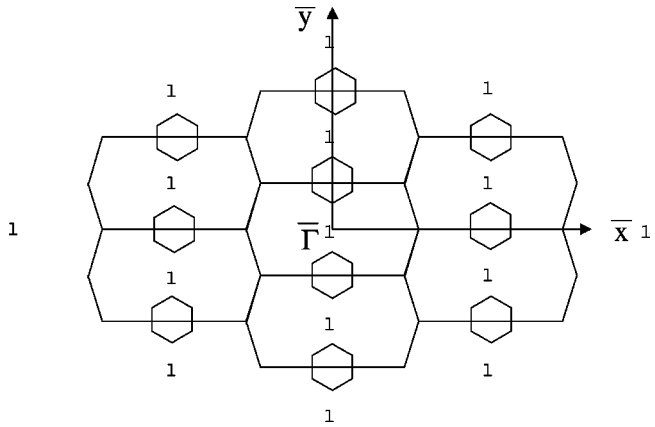

FIG. 4. Representation of the surface Brillouin zone (SBZ) for the 1×1 fcc(113) surface. The dots are the projection of the reciprocal space in the (113) plane. $\bar{x}$ and $\bar{y}$ are the $[\bar{1}10]$ and $[33\bar{2}]$, directions, respectively. The hexagons represent the location of the energy gaps above the Fermi level in *k* space. Starting from $\bar{\Gamma}$ and going along $\bar{x}$, there is an energy gap beyond the SBZ boundary. This same gap can also be reached along the $\bar{y}$ direction. The projected electronic structure of Figs. 1 and 2 show the actual extent of this gap in each direction.

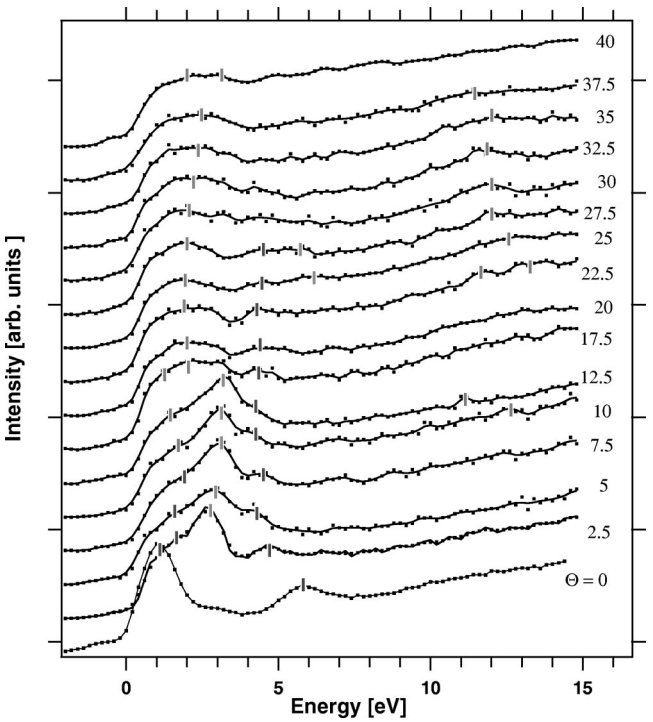

FIG. 5. Superposition of a set of IPS spectra. They display the photon flux intensity as a function of the energy of the incoming electrons. The square symbols correspond to the actual data. The thin line is a smoothed spline to guide the eye. Several surface resonances have been highlighted with vertical lines.

IV. EXPERIMENTAL RESULTS AND DISCUSSION

A. $[\bar{1}10]$ direction

We will consider first a set of spectra along the direction of the close-packed rows ($[\bar{1}10]$ direction). Since the reconstruction of the surface shows no change in the surface periodicity along this direction, as judged from the LEED diagrams, one should not expect a large influence of the atomic rearrangement on the surface electronic structure. Figure 5 shows a series of IPS spectra for different angles of the incoming electrons with respect to the surface normal. The Fermi level is clearly distinguishable as the onset for the photon intensity, and it has been used as the zero for the energy scale. The intensity is measured as photons/(electrons × energy), but they are presented in an arbitrary scale. Some of the spectra have been rescaled to facilitate display.

There are clearly two sets of resonances, one of them located 10 eV above ε_F and the other just below 5 eV. The high-energy resonances are fairly weak in intensity, and show very little dispersion in energy. The low-energy resonances are instead fairly well defined, which makes the identification of their evolution easier, as the angle with respect

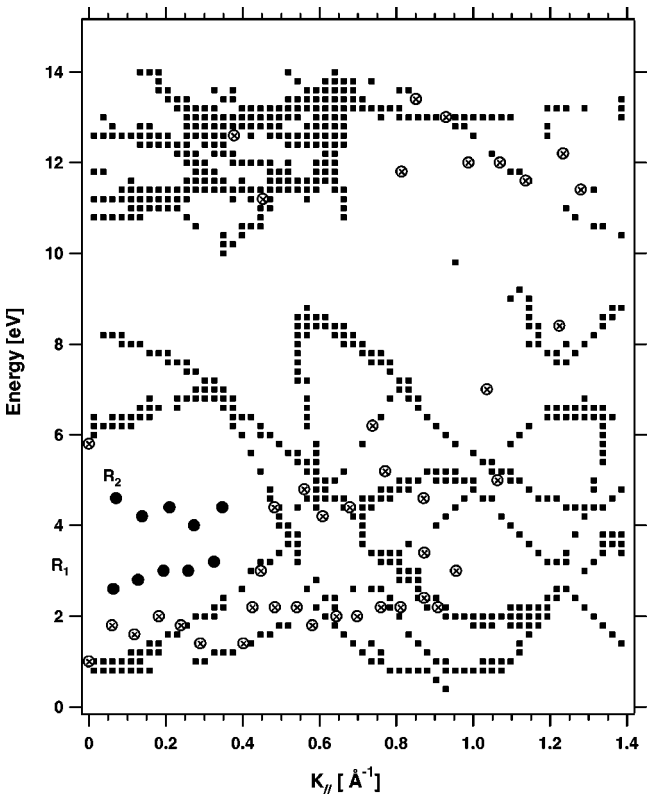

FIG. 6. Dispersion of the surface resonances as a function $k_{//}$ along $[\bar{1}10]$. The experimental data are shown by circles ($\otimes$ and $\bullet$). The theoretical prediction for bulk-derived transitions are labeled by the filled squares. R_1 and R_2 are surface resonances. See the text for further details.

to the surface normal is changed. Also these states disperse over a wider energy range, as can be seen directly from Fig. 5.

In Fig. 6 we show a plot of ε vs $k_{//}$ for this particular azimuth (parallel momentum along the $[\bar{1}10]$ direction). The filled squares are the results of a numerical calculation of possible direct bulk transitions. They represent the energy and momentum of a final state for a transition from an energy state 9.5 ± 0.3 eV higher at the same value of k, using the bulk energy bands calculated as described in Sec. III. This way of finding the transitions is more realistic than using the parabolic approximation of the final state to map the energy dispersion of a particular spectral feature. The value 9.5 eV matches the IPS's detector response. We have added a 0.3-eV Gaussian noise to mimic the experimental response. This calculation does not include the matrix element effects on the optical transitions, which will likely drive some of the predicted events below the detectability limit.

The circular data markers in Fig. 6 come from the measured data (Fig. 5), and correspond to the different resonances in each spectrum. We have chosen to separate them into two groups: one includes all data points that superimpose with calculated values of bulk derived features ($\otimes$), while the other set comprises those clearly located in a gap ($\bullet$) of the allowed bulk transitions.

It should be clear that there is no absolute gap along this azimuth; the open areas in the $\varepsilon - k_{//}$ plane, shown in Fig. 6, are related to the restrictions on energy and momentum imposed on the bulk transitions. We can then associate several resonances with bulk-derived features. At the same time, we can recognize the existence of surface resonances, most notably those labeled R_1 and R_2, since they show no correlation with the calculated transitions. Rigorously they cannot be labeled as surface states, since their energies are not in a gap of the bulk energy bands. R_2, at 4.4 eV, could be attributed to an image state, since it is always below the vacuum level, but it has a fairly flat dispersion with $k_{//}$. The second resonance R_1 at about 2.4 eV above ε_F, has a binding energy which is too large for this state to be a lower-energy state of the Rydberg series of image states. Image states are usually confined within 1 eV of the vacuum level. This argument is confirmed by a calculation we performed following Smith *et al.*[26] for the image states predicted by the Jones-Jennings-Jepsen (JJJ)[25] potential. Using parameters similar to those used to fit image states on the Au(100) surface ($U_o=1.25$ Ry, $z_o=2.8$ a.u., and $\lambda=2.3$ a.u.; see Ref. 24), we obtained the following binding energies measured with respect to the vacuum level for the first three states: $\varepsilon_0=10.3$ eV, $\varepsilon_1=0.8$ eV, and $\varepsilon_2=0.2$ eV. The first energy is below ε_F, so it is an occupied state, which cannot be observed using IPS. The next two states are at 4.5 and 5.1 eV above ε_F. For this set of parameters the energy of the second state compares well with those measured for R_2, making it reasonable to assign it as an image resonance, but they do not simultaneously fit the energy of R_1.[27] This indicates that R_1 cannot be assigned as an image resonance. To find its origin, a more detailed calculation of the surface electronic structure should be done.

B. $[33\bar{2}]$ direction

In Fig. 7 we show a complete set IPS spectra for the $[33\bar{2}]$ azimuth. We can clearly identify several resonances with large dispersions, in some cases spanning an energy range as large as 2 eV.

At low angles there are two prominent resonances in the spectra. One of them starts dispersing toward the Fermi level from about 6 eV at normal incidence, down to 4 eV about 15° off normal. Another resonance starts from 1.3 eV above the Fermi level at normal incidence, increasing its energy up to 2.9 eV at about 17.5°. At 30° a resonance emerges (S) at about 3 eV, and as the angle increases it moves toward the Fermi level, arriving at a minimum energy at about 40°. For larger angles it moves back to higher energies, and can be clearly detected as far as 55° off normal. We have represented all these resonances in a ε vs $k_{//}$ plot in Fig. 8. The dark circular markers are data points taken from the IPS spectra, and the black squares are again the theoretical predictions for the bulk-allowed transitions. In addition, in a solid line we have encircled the region of the absolute energy gap for this azimuth, as determined from our calculation shown in Fig. 2.

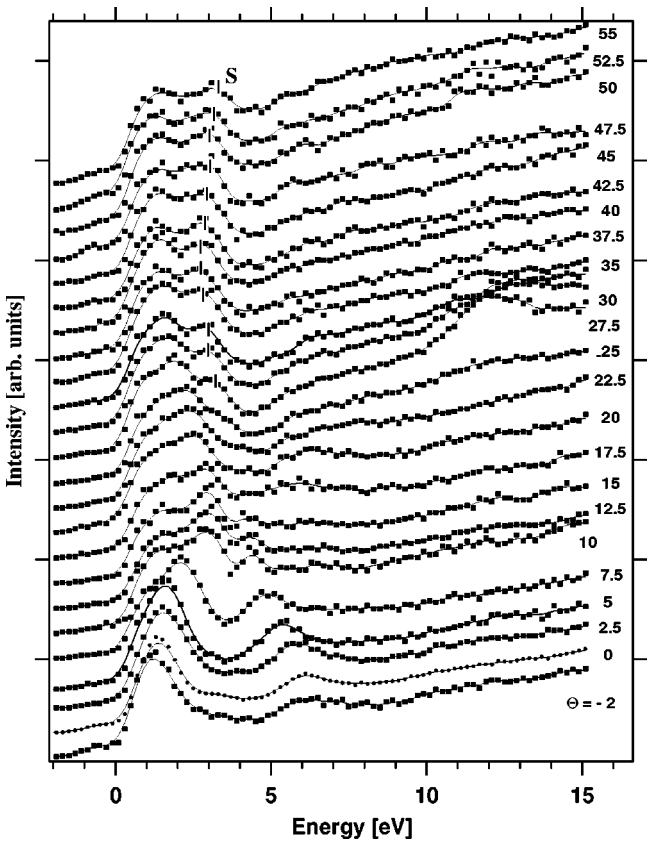

FIG. 7. IPS spectra along the $[33\bar{2}]$ direction. Measured data points are the solid squares. The resonance labeled by *S* is a surface state.

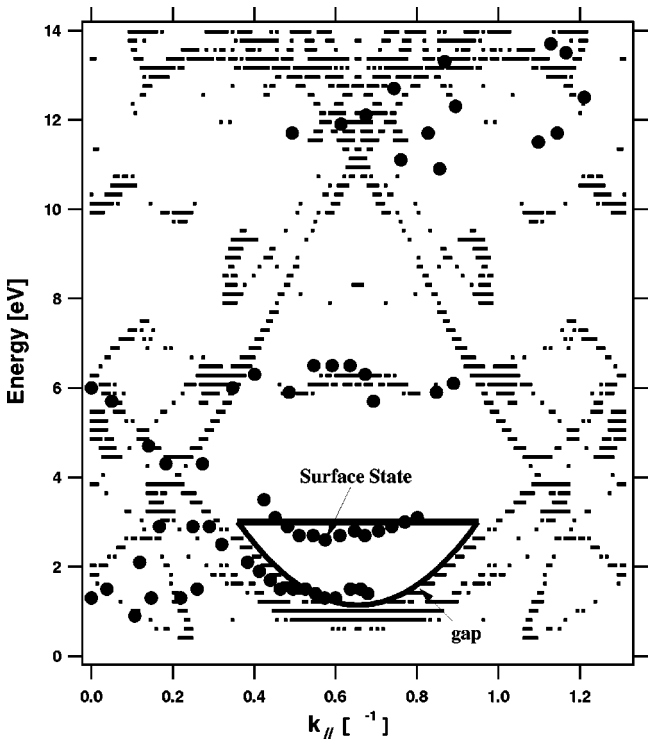

FIG. 8. Experimental resonances (●) and bulk predicted transitions (black squares) along the $[33\bar{2}]$ direction. The surface state (*S*) is clearly contained in the gap.

Most of the experimental data points are on top of the bulk-allowed transition, and closely follow the dispersion of the calculated features. An exception to this statement is the state labeled *S*, which is in an absolute energy gap, so we can legitimately call it a surface state. The differences between the nature of *S* and the resonances along the $[\bar{1}10]$ direction, R_1 and R_2, are subtle but clear. The latter are contained in a ''spectrometer gap.'' This means that, for a different energy of the emitted photons (fixed by the detector's gas-window combination), there are bulk final states with the same energies as the resonances. *S* is contained within an absolute band gap, where no bulk states exists. Also, the energy dispersion of *S* clearly follows the symmetry of the nearby energy bands, distinguishing it from an image-charge-type state which has its minimum energy at $\bar{\Gamma}$. The surface state *S* has its minimum energy at the zone boundary: $k_{//}=0.66$ Å^{-1}.

V. CONCLUSIONS

Using IPS, we have studied the empty electronic states of Au(113) from the Fermi level up to 15 eV along the two main crystallographic axes $[\bar{1}10]$ and $[33\bar{2}]$. In addition, from first principles, we calculated the Au band structure. We used this information to perform a surface projection of the bulk electronic structure, and determined the location of the surface energy gaps. Comparing the experimental results with the transitions predicted by our calculation we were able to recognize several surface resonances. Some of these were derived from bulk states. From calculations we gained insight into the nature and origin of one of the surface resonances (along the $[\bar{1}10]$ direction), and we were able to clearly recognize a surface state (along the $[33\bar{2}]$ direction, with a minimum energy of 2.7 eV at $k_{//}\approx 0.6$ Å^{-1}).

ACKNOWLEDGMENTS

We thank Dr. Dave Zehner for his help in preparing the crystal. This research received financial support from FONDECYT, Grant Nos. 1990812 and 1990304, Fundación Andes Grant No. C-10810/2, and ICM P99-135F.

*Email address: phaberle@fis.utfsm.cl

[1] D. P. Wooddruff, N. V. Smith, P. D. Johnson, and W. A. Roger, Phys. Rev. B **26**, 2943 (1982).

[2] B. Reihl, K. H. Frank, and R. Schlittler, Phys. Rev. Lett. **52**, 1826 (1984).

[3] R. A. Bartynski, T. Gustafsson, and P. Soven, Phys. Rev. B **31**, 4745 (1985).

[4] A. Goldman, V. Dose, and G. Borstel, Phys. Rev. B **32**, 1971 (1985).

[5] N. V. Smith, Phys. Rev. B **32**, 3549 (1985).

[6] C. T. Chen and N. V. Smith, Phys. Rev. B **40**, 7487 (1989).
[7] *Unoccupied Electronic States*, edited by J. C. Fuggle and J. E. Inglesfield (Springer-Verlag, Berlin, 1992).
[8] F. Ciccacci, S. De Rossi, A. Taglia, and S. Crampin, J. Phys.: Condens. Matter **6**, 7227 (1994).
[9] D. Straub and F. J. Himpsel, Phys. Rev. Lett. **52**, 1922 (1984).
[10] D. P. Woodruff, W. A. Roger, and N. V. Smith, Phys. Rev. B **34**, 764 (1986).
[11] R. A. Bartynski and T. Gustafsson, Phys. Rev. B **33**, 6588 (1986).
[12] F. J. Himpsel, Phys. Rev. B **44**, 5966 (1991).
[13] S. Crampin, S. de Rossi, and F. Ciccacci, Phys. Rev. B **53**, 13 817 (1996).
[14] D. Arena, F. Curti, and R. Bartynski, Phys. Rev. B **56**, 15 404 (1997).
[15] J. B. Pendry, J. Phys. C **14**, 1381 (1981).
[16] G. Denninger, V. Dose, and H. Scheidt, Appl. Phys. **18**, 375 (1979).
[17] P. Erdman and E. Zipf, Rev. Sci. Instrum. **53**, 225 (1982).
[18] P. Häberle, Phys. Low-Dimens. Semicond. Struct. **10/11**, 317 (1995).
[19] F. Meier and D. Pescia, Phys. Rev. Lett **47**, 374 (1981).
[20] M. Sotto and J. C. Boulliuard, Surf. Sci. **214**, 97 (1989).
[21] Q. T. Jiang, T. Gustafsson, P. Häberle, and D. M. Zehner, Phys. Rev. B **45**, 14 256 (1992).
[22] A. Sandy, Ph.D. thesis, MIT, Cambridge, MA, 1992.
[23] O.K. Andersen and O. Jepsen, Phys. Rev. Lett. **53**, 2551 (1984); O. K. Andersen, O. Jepsen, and D. Gloetzel, in *Highlights of Condensed Matter Theory*, edited by F. Bassani, F. Fumi, and M. P. Tosi (North-Holland, New York, 1985); O. K. Andersen, O. Jepsen, and M. Sob, in *Lecture Notes in Physics: Electronic Band Structure and Its Applications*, edited by M. Yussouff (Springer-Verlag, Berlin, 1987).
[24] See, for instance, *Electron States and Fermi Surfaces of Elements*, edited by K. H. Hellwege and O. Madelung, Landölt-Börnstein, New Series, Group III, Vol. 13, Pt. c (Springer-Verlag, Berlin, 1999), and references therein.
[25] R. Jones, P. Jennings, and O. Jepsen, Phys. Rev. B **29**, 6474 (1984).
[26] N. Smith, C. Chen, and W. Weinert, Phys. Rev. B **40**, 7565 (1989).
[27] For completeness, it should be added that we have obtained an almost perfect agreement between the predictions of the JJJ model for image states and the measured energies of R_1 and R_2, using the standard values of U_o, λ, and z_o, but for $m=4m_0$. At this time we have no reasonable explanation for why Au(113) could induce such a large increase in the effective electron mass. An effect like this should in principle be present in all other low-index surfaces of Au, but no other measurement has shown evidence of it.